JOURNAL OF GUIDANCE, CONTROL, AND DYNAMICS
Vol. 32, No. 2, March–April 2009

Modeling of Generic Slung Load System

Morten Bisgaard,* Jan Dimon Bendtsen,† and Anders la Cour-Harbo†
Aalborg University, 9220 Aalborg, Denmark

DOI: 10.2514/1.36539

This paper presents the annotated result of the modeling and verification of a generic slung-load system using a small-scale helicopter. The model is intended for use in simulation, pilot training, estimation, and control. The model is derived using a redundant coordinate formulation based on Gauss's Principle of Least Constraint using the Udwadia–Kalaba equation and can be used to model all body-to-body slung-load suspension types. The model provides intuitive and easy-to-use means of modeling and simulating different slung-load suspension types. It includes detection of, and response to, wire slackening and tightening, as well as aerodynamic coupling between the helicopter and the load. Furthermore, it is shown how the model can be easily used for multilift systems, either with multiple helicopters or multiple loads. A numerical stabilization algorithm is introduced, and, finally, the use of the model is illustrated through simulations and flight verifications.

Nomenclature

$\boldsymbol{A}$	=	Jacobian of the constraint function
$\boldsymbol{a}$	=	translational acceleration vector
$\boldsymbol{b}$	=	acceleration independent part of constraint function
c_d	=	numerical correction damper constant
D	=	area
$\boldsymbol{F}$	=	force vector
$\boldsymbol{g}$	=	constraint equation
$\boldsymbol{I}$	=	inertia tensor
J	=	impulse
k_s	=	numerical correction spring constant
$\boldsymbol{L}$	=	wire vector
$\boldsymbol{M}$	=	generalized mass matrix (positive symmetric definite)
m	=	mass
$\boldsymbol{N}$	=	normalized wire vector
$\boldsymbol{Q}$	=	generalized forces
$\boldsymbol{q}$	=	generalized coordinates
$\boldsymbol{R}$	=	position vector, $[x \quad y \quad z]^T$
R	=	rotor radius
$\boldsymbol{T}_{\theta b}$	=	mapping of angular rates to Euler velocities
$\boldsymbol{T}_{be}$	=	transformation matrix from e to b
$\boldsymbol{v}$	=	translational velocity vector
v_w	=	induced inflow
W	=	length of taut wire
χ_w	=	wake-skew angle
$\dot{\boldsymbol{x}}$	=	time derivative of the vector $\boldsymbol{x}$
$\tilde{\boldsymbol{x}}$	=	skew symmetric matrix used for cross-product operation with the vector $\boldsymbol{x}$
$\boldsymbol{\alpha}$	=	angular acceleration vector
δ	=	drag coefficient
$\boldsymbol{\theta}$	=	Euler angle collection, $[\phi \quad \theta \quad \psi]^T$
λ	=	induced inflow ratio
μ	=	rotor advance ratio
$\boldsymbol{\tau}$	=	torque vector
$\boldsymbol{\omega}$	=	angular velocity vector

Subscripts

b	=	general body coordinate system
c	=	constrained
e	=	Earth-fixed coordinate system
h	=	helicopter body coordinate system
i	=	wire number
j	=	helicopter number, in multilift systems
l	=	load body coordinate system
m	=	number of constraints
n	=	number of system coordinates
u	=	unconstrained
w	=	wake
1	=	before wire tightening
2	=	after wire tightening

I. Introduction

HELICOPTERS carrying external suspended loads (underslung loads) have been the focus of significant interest in the aerospace research community for the last 40 years due to the inherent stability problems from which such systems suffer [1–5]. Most of the research has been focused on stability analysis to determine favorable system parameters like wire lengths, helicopter/load mass ratios, etc., as well as designing stability augmenting techniques for slung-load systems. Most models developed in this research have been simple and situation specific and, although a small number of publications have been focused on more general models suited for both simulation and control, this is not a thoroughly researched field. The main contribution of this paper is to present a new approach to modeling a generic slung-load system that is able to handle both multilift systems and wire slackening and tightening.

The specific focus for the model is simple simulation, online estimation, and controller design, and it is derived using a redundant coordinate formulation. This means that the two-body problem is treated as a 12 degree-of-freedom (DOF) setup and constraints imposed by the wires are modeled as forces. Wires are modeled as inelastic, as opposed to elastic. This is due to the fact that this project is on small unmanned aerial vehicle (UAV) systems with low mass, where the wires used are stiff compared to the situation with full-scale systems, where it is often necessary to consider wire elasticity.

The derivation of the model is based on Gauss's Principle of Least Constraint using the Udwadia–Kalaba equation, which is a recently developed approach for modeling constrained dynamical systems. The derived model is simple and intuitive, and it is capable of directly modeling all body-to-body slung-load suspension types like the inverted-V system. For suspension systems where wires are not body-to-body, like the inverted-Y and systems with spreader bars, the model can handle these by introducing small masses in the wire connections.

Presented as Paper 6816 at the AIAA Modeling and Simulation Technologies Conference and Exhibit, Keystone, CO, 21–24 August 2006; received 8 January 2008; accepted for publication 1 September 2008.

*Assistant Professor, Department of Electronic Engineering, Section for Automation and Control, Fredrik Bajers Vej 7C.

†Associate Professor, Department of Electronic Engineering, Section for Automation and Control, Fredrik Bajers Vej 7C.

It should be noted that two different modeling approaches exist: a minimal and a redundant formulation. A minimal formulation describes the problem in terms of degrees of freedom and generalized coordinates. This leads to a minimal set of equations that does not reveal the constraint forces. The redundant formulation, on the other hand, expresses the system in terms of redundant coordinates and constraint forces.

The redundant formulation is used in this model, yielding the advantage that it is easy to change the suspension system; this is simply done by changing the constraint equations. Furthermore, it makes it possible to effortlessly remove and add constraints, which are used in the wire slackening and tightening modeling. A disadvantage is that numerical integration errors will accumulate in the model; this is addressed in this work by the introduction of a numerical correction scheme.

One of the very first to consider the dynamics of an object being towed through air was Glauert in 1930 [6], and he discovered the stability problems involved in such a task. He identified that short wires and low load mass were factors that could lead to instabilities of the slung-load system. The first study in a complete helicopter slung-load system was performed by Lucassen and Sterk [7]. Their analysis was limited to 3-degrees-of-freedom (DOF) hover and excluded load aerodynamics, but was nevertheless the first to consider the coupling between helicopter and slung load. In the following two decades, a large number of different researchers have considered the stability of slung-load systems through analytical studies as well as experimental testing. Almost all studies have focused on determining a stable region of flight with respect to slung-load parameters to avoid instabilities [1–4,8]. Some have analyzed certain parameters such as the shape of the load itself to reduce instabilities, including considering different stabilizing implements like gyroscopes, fins, and drogues [9,10].

Common for most of the models developed in these studies is that they are somewhat limited and focused directly on stability analysis in a bounded region. Poli and Cromack presented a 10-state linearized model, which assumed no coupling of lateral and longitudinal motion [1]. The model only dealt with single-point suspension and forward flight, and the study concluded that a long wire is needed for stability, but it also concluded (contrary to Glauert [6]) that a low load mass is a requirement for stability. Studies have shown that it is beneficial to use gyroscopes and fins to stabilize the load [9]. Experimental tests using forced oscillations in a wind tunnel to obtain stability information have also been performed [10]. The dynamic and flowfield of the helicopter were ignored and the conclusion was that a two-wire suspension system solved some of the single-wire stability problems.

A more extensive model was developed by Prabhakar in which Newton–Euler equations were used to describe an inverted-V suspension system and included a helicopter model based on stability derivatives [2]. The model assumed inflexible and inextensible wires and described the system by a minimal coordinate formulation constraining the full 12-degrees-of-freedom system to nine. It was noted that it was difficult to obtain an adequate model of yaw motion.

A major work was the Ph.D. thesis by Sampath, who was one of the first to use a Lagrange formulation that formed a complete set of 12-degrees-of-freedom equations, which included all body-to-body suspension schemes, like the inverted-V, but not the inverted-Y [3]. Aerodynamic models of both helicopter and load were included as well as wires implemented as extensible springs with viscous damping. The possibility of wire slackening was also modeled, but not wire tightening. A Newtonian approach was applied by Ronen et al. to develop a full model of single-point suspension systems, where rotor downwash on the load as well as unsteady aerodynamics of the load were taken into account [4].

One of the most comprehensive treatments of slung-load modeling can be found in [5,11], where specific simulation models for different kinds of single- and multiple-point suspension systems, as well as multilift systems (more than one helicopter), were developed. Both suspension systems with elastic and inelastic wires were treated using an explicit constraint method that separates the motion due to the wire stretching from the motion due to the coupled rigid-body dynamics. In a recent publication, the single-point suspension-type models found in [5] have been implemented and simulated [12].

For an elaborate survey of the different research in this area, see Sampath's thesis [3] where many older references dealing with different kinds of stability analyses have been treated.

The paper is organized as follows. First, the Udwadia–Kalaba modeling principle is introduced, and the principle is then used to derive the actual model. The model is then augmented with wire slackening and tightening, and, in Sec. V, it is shown how the model can be used to model multilift systems with multiple helicopters and loads. Aerodynamic coupling between helicopter and slung load is introduced into the model in Sec. VI, and numerical model stability is discussed in Sec. VII. Finally, use of the model is presented through simulation in Sec. VIII and through flight verification in Sec. IX.

II. Udwadia–Kalaba Equation

Recently, a new perspective on constraint systems yielded a new principle of dynamic system modeling [13]. The Udwadia–Kalaba principle is based on Gauss's principle of least constraint and yields an explicit equation for calculation of the dynamics. It seems to be simpler to use than other approaches such as Hamiltonian equations, but it should be noted that the principles of Lagrange and Udwadia–Kalaba are equivalent [14].

As a starting point, an unconstrained Newtonian system

$$\boldsymbol{M}\,\ddot{\boldsymbol{q}}_u = \boldsymbol{Q} \tag{1}$$

consisting of a number of rigid bodies with 6-DOF each, is considered. $\boldsymbol{M} \in \mathbb{R}^{n\times n}$ is the positive definite symmetric generalized mass matrix, $\boldsymbol{q}_u \in \mathbb{R}^n$ is a vector containing the unconstrained generalized coordinates of the system, and $\boldsymbol{Q} \in \mathbb{R}^n$ is a vector representing the generalized forces acting on the system. The system is then subjected to m constraints, which do not need to be independent and can be either holonomic (position dependent) or nonholonomic (position and velocity dependent), of the form

$$\boldsymbol{g}(\boldsymbol{q}, t) = 0, \qquad \boldsymbol{g}(\boldsymbol{q}, \dot{\boldsymbol{q}}, t) = 0 \tag{2}$$

where $\boldsymbol{q} \in \mathbb{R}^n$ are the generalized coordinates of the constrained system. Under the assumption that the constraints are sufficiently smooth, they can then be differentiated either twice or once, respectively, to yield

$$\boldsymbol{A}(\boldsymbol{q}, \dot{\boldsymbol{q}}, t)\ddot{\boldsymbol{q}} = \boldsymbol{b}(\boldsymbol{q}, \dot{\boldsymbol{q}}, t) \tag{3}$$

where $\boldsymbol{A} \in \mathbb{R}^{m\times n}$ is the Jacobian of the constraint function (2) and $\boldsymbol{b} \in \mathbb{R}^m$ is the acceleration independent part of the constraint equation. It can be noted that Eq. (3) is equivalent to Eq. (2) when used together with a set of inertial conditions that satisfy the constraints.

To transform the original Newtonian system into a constrained system, Eq. (1) is augmented with a constraint force ($\boldsymbol{Q}_c \in \mathbb{R}^n$)

$$\boldsymbol{M}\,\ddot{\boldsymbol{q}} = \boldsymbol{Q} + \boldsymbol{Q}_c \tag{4}$$

which means that the motion of the constraint system originates both from the external forces as well as the constraints. Using the Udwadia–Kalaba equation [13], it is possible to calculate the constraint forces of Eq. (4) in the following way:

$$\boldsymbol{Q}_c = \boldsymbol{M}^{1/2}(\boldsymbol{A}\boldsymbol{M}^{-1/2})^{+}(\boldsymbol{b} - \boldsymbol{A}\ddot{\boldsymbol{q}}_u) \tag{5}$$

through the use of the Moore–Penrose pseudoinverse (denoted by $+$). This yields the following dynamic equation for the constrained system

$$\ddot{\boldsymbol{q}} = \ddot{\boldsymbol{q}}_u + \boldsymbol{M}^{-1/2}(\boldsymbol{A}\boldsymbol{M}^{-1/2})^{+}(\boldsymbol{b} - \boldsymbol{A}\ddot{\boldsymbol{q}}_u) \tag{6}$$

III. Rigid-Body Modeling

The rigid-body modeling of the entire helicopter/slung-load system will be done in a similar manner as the usual approach for a single rigid body, using the Udwadia–Kalaba Eq. (6) to calculate the acceleration of the system.

The rigid-body model is derived with respect to an inertially fixed reference frame denoted as the Earth-fixed frame ${}^{e}(\cdot)$ oriented with the z axis pointing down, x axis point north, and y axis pointing east. Body-fixed coordinate systems are defined at the center of mass (c.m.) for each object present in the system, that is, one for the helicopter ${}^{h}(\cdot)$ and one for the slung load ${}^{l}(\cdot)$. A generalized body-fixed frame is denoted as ${}^{b}(\cdot)$. All reference frames used are right-hand Cartesian coordinate systems.

The angular and translational motion of a rigid body can be described as [15]

$$ {}^{b}\dot{\boldsymbol{v}}_b = m_b^{-1\,b}\boldsymbol{F}_b - {}^{b}\tilde{\boldsymbol{\omega}}_b\,{}^{b}\boldsymbol{v}_b = {}^{b}\boldsymbol{a}_b - {}^{b}\tilde{\boldsymbol{\omega}}_b\,{}^{b}\boldsymbol{v}_b \tag{7} $$

$$ {}^{b}\dot{\boldsymbol{\omega}}_b = \boldsymbol{I}_b^{-1\,b}\boldsymbol{\tau}_b - \boldsymbol{I}_b^{-1\,b}\tilde{\boldsymbol{\omega}}_b\boldsymbol{I}_b\,{}^{b}\boldsymbol{\omega}_b = {}^{b}\boldsymbol{\alpha}_b - \boldsymbol{I}_b^{-1\,b}\tilde{\boldsymbol{\omega}}_b\boldsymbol{I}_b\,{}^{b}\boldsymbol{\omega}_b \tag{8} $$

where ${}^{b}\boldsymbol{a}_b$, ${}^{b}\boldsymbol{\alpha}_b$ are specific applied forces and torques, ${}^{b}\boldsymbol{v}_b$ is body-fixed translational velocity, ${}^{b}\boldsymbol{\omega}_b$ is body-fixed angular velocity, and $\boldsymbol{I}_b$ is the inertia tensor of the body. Index b is used to indicate a generic rigid body.

Integration of Eqs. (7) and (8) yields the body velocities, which can then be transformed into the Earth-fixed frame to be integrated once more to yield the position and Euler angles

$$ {}^{e}\boldsymbol{v}_b = \boldsymbol{T}_{eb}\,{}^{b}\boldsymbol{v}_b \tag{9} $$

$$ \dot{\boldsymbol{\theta}}_b = \boldsymbol{T}_{\theta b}\,{}^{b}\boldsymbol{\omega}_b \tag{10} $$

where the transformation matrix $\boldsymbol{T}_{eb}$: $\mathbb{R}^3 \to \mathbb{R}^3$ is the orthogonal transformation that maps from the body to the Earth frame. The transformation matrix $\boldsymbol{T}_{\theta b}$: $\mathbb{R}^3 \to \mathbb{R}^3$ relates the body angular velocities to the Euler velocities. This approach is illustrated in Fig. 1 using the generalized coordinates. Because a redundant approach to the rigid-body modeling is used, the Earth-fixed generalized coordinates are chosen to be

$$ \boldsymbol{q} = \begin{bmatrix} {}^{e}\boldsymbol{R}_h \\ \boldsymbol{\theta}_h \\ {}^{e}\boldsymbol{R}_l \\ \boldsymbol{\theta}_l \end{bmatrix}_{12\times 1} \qquad {}^{e}\boldsymbol{R}_b = \begin{bmatrix} {}^{e}x_b \\ {}^{e}y_b \\ {}^{e}z_b \end{bmatrix} \qquad \boldsymbol{\theta}_b = \begin{bmatrix} \phi_b \\ \theta_b \\ \psi_b \end{bmatrix} \tag{11} $$

The body-fixed generalized coordinates then become

$$ \dot{\boldsymbol{q}}_b = \begin{bmatrix} {}^{h}\boldsymbol{v}_h \\ {}^{h}\boldsymbol{\omega}_h \\ {}^{l}\boldsymbol{v}_l \\ {}^{l}\boldsymbol{\omega}_l \end{bmatrix}_{12\times 1} \qquad {}^{b}\boldsymbol{v}_b = \begin{bmatrix} {}^{b}v_{x_b} \\ {}^{b}v_{y_b} \\ {}^{b}v_{z_b} \end{bmatrix} \qquad {}^{b}\boldsymbol{\omega}_b = \begin{bmatrix} {}^{b}\omega_{x_b} \\ {}^{b}\omega_{y_b} \\ {}^{b}\omega_{z_b} \end{bmatrix} \tag{12} $$

A. Constraint Equation

To solve the Udwadia–Kalaba equation in the rigid-body model, it is necessary to determine the constraints in the form of Eq. (3) (i.e., finding $\boldsymbol{A}$ and $\boldsymbol{b}$), which will be demonstrated in this section. The general configuration of the slung-load system is illustrated in Fig. 2

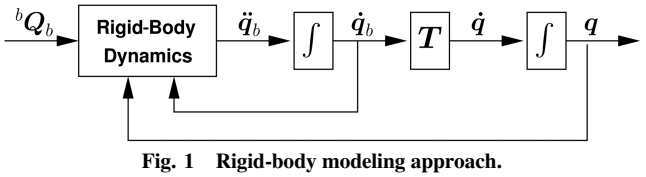

Fig. 1 Rigid-body modeling approach.

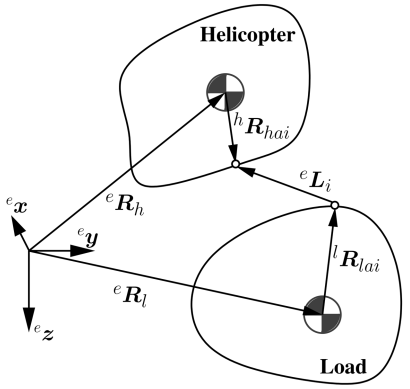

Fig. 2 General configuration of the slung-load system shown for the *i*th wire.

where the ith wire is shown. The nominal configuration for the system is considered to be with a taut wire. The ith wire vector ${}^{e}\boldsymbol{L}_i$ is given by

$$ \begin{aligned} {}^{e}\boldsymbol{L}_i &= {}^{e}\boldsymbol{R}_h + {}^{e}\boldsymbol{R}_{\text{hai}} - {}^{e}\boldsymbol{R}_l - {}^{e}\boldsymbol{R}_{\text{lai}} \\ \Leftrightarrow\ {}^{e}\boldsymbol{L}_i &= {}^{e}\boldsymbol{R}_h + \boldsymbol{T}_{eh}\,{}^{h}\boldsymbol{R}_{\text{hai}} - {}^{e}\boldsymbol{R}_l - \boldsymbol{T}_{el}\,{}^{l}\boldsymbol{R}_{\text{lai}} \end{aligned} \tag{13} $$

that is, a function of the position vectors of the helicopter and the load (${}^{e}\boldsymbol{R}_h$ and ${}^{e}\boldsymbol{R}_l$) as well as the static position vectors describing the attachment points on the helicopter and the load (${}^{h}\boldsymbol{R}_{\text{hai}}$ and ${}^{l}\boldsymbol{R}_{\text{lai}}$).

To transform this constraint equation into the general form of Eq. (3), it needs to be differentiated twice. In connection with this, it is important to note that the wire vector is unknown in this case and it is therefore desirable to cancel it from the equation. This can be achieved by working with the norm of ${}^{e}\boldsymbol{L}_i$ instead of the vector itself, as the length of the wire is constant and will vanish during the differentiation. This yields

$$ g_i(\boldsymbol{q}) = \|{}^{e}\boldsymbol{L}_i\|^2 - W_i^2 = ({}^{e}\boldsymbol{L}_i)^T({}^{e}\boldsymbol{L}_i) - W_i^2 \tag{14} $$

where W_i is the nominal undeformed, taut length of the wire. In the following, the notation is now eased by dropping the coordinate system indices on the position vectors, that is, it is implicit that the position vector of the ith attachment on the load is given in the load frame, etc.

To achieve the standard form of Eq. (3), the constraint Eq. (14) is differentiated twice

$$ \dot{g}_i(\boldsymbol{q}) = 0 = 2\dot{\boldsymbol{L}}_i^T\boldsymbol{L}_i \tag{15} $$

$$ \ddot{g}_i(\boldsymbol{q}) = 0 = 2\ddot{\boldsymbol{L}}_i^T\boldsymbol{L}_i + 2\dot{\boldsymbol{L}}_i^T\dot{\boldsymbol{L}}_i \tag{16} $$

where

$$ \dot{\boldsymbol{L}}_i = \dot{\boldsymbol{R}}_h - \dot{\boldsymbol{R}}_l + \dot{\boldsymbol{T}}_{eh}\boldsymbol{R}_{\text{hai}} - \dot{\boldsymbol{T}}_{el}\boldsymbol{R}_{\text{lai}} \tag{17} $$

$$ \ddot{\boldsymbol{L}}_i = \ddot{\boldsymbol{R}}_h - \ddot{\boldsymbol{R}}_l + \ddot{\boldsymbol{T}}_{eh}\boldsymbol{R}_{\text{hai}} - \ddot{\boldsymbol{T}}_{el}\boldsymbol{R}_{\text{lai}} \tag{18} $$

Using the relationship [15]

$$ \begin{aligned} &\dot{\boldsymbol{T}}_{eb} = \boldsymbol{T}_{eb}\,{}^{b}\tilde{\boldsymbol{\omega}}_b \Rightarrow \\ &\ddot{\boldsymbol{T}}_{eb} = \dot{\boldsymbol{T}}_{eb}\,{}^{b}\tilde{\boldsymbol{\omega}}_b + \boldsymbol{T}_{eb}\,{}^{b}\dot{\tilde{\boldsymbol{\omega}}}_b = \boldsymbol{T}_{eb}\,{}^{b}\tilde{\boldsymbol{\omega}}_b\,{}^{b}\tilde{\boldsymbol{\omega}}_b + \boldsymbol{T}_{eb}\,{}^{b}\dot{\tilde{\boldsymbol{\omega}}}_b \end{aligned} \tag{19} $$

together with Eq. (9), we can express Eq. (17) as

$$ \dot{\boldsymbol{L}}_i = \boldsymbol{T}_{eh}\,{}^{h}\boldsymbol{v}_h - \boldsymbol{T}_{el}\,{}^{l}\boldsymbol{v}_l + \boldsymbol{T}_{eh}\,{}^{h}\tilde{\boldsymbol{\omega}}_h\boldsymbol{R}_{\text{hai}} - \boldsymbol{T}_{el}\,{}^{l}\tilde{\boldsymbol{\omega}}_l\boldsymbol{R}_{\text{lai}} \tag{20} $$

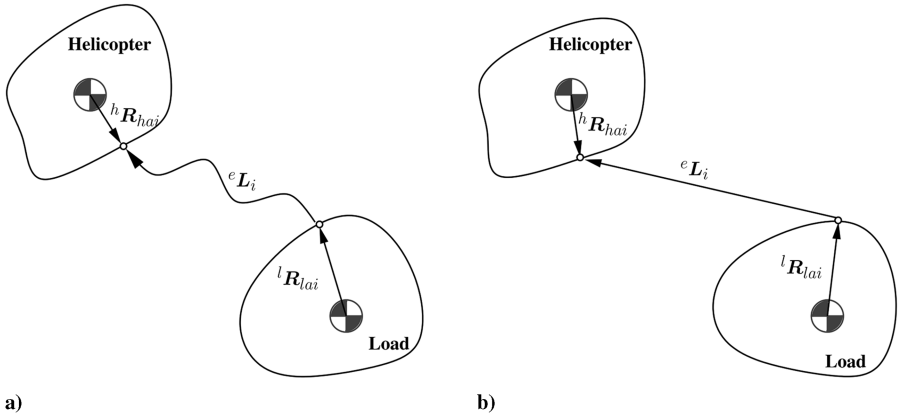

Fig. 3 Situations with a) slack wire and b) taut wire.

Similarly, Eq. (18) can be expressed as

$$\begin{aligned}\ddot{\boldsymbol{L}}_i &= \boldsymbol{T}_{eh}{}^{h}\boldsymbol{a}_h - \boldsymbol{T}_{el}{}^{l}\boldsymbol{a}_l + \boldsymbol{T}_{eh}{}^{h}\tilde{\boldsymbol{\omega}}_h{}^{h}\tilde{\boldsymbol{\omega}}_h{}^{h}\boldsymbol{R}_{\text{hai}} - \boldsymbol{T}_{el}{}^{l}\tilde{\boldsymbol{\omega}}_l{}^{l}\tilde{\boldsymbol{\omega}}_l{}^{l}\boldsymbol{R}_{\text{lai}} \\ &+ \boldsymbol{T}_{eh}{}^{h}\dot{\tilde{\boldsymbol{\omega}}}_h{}^{h}\boldsymbol{R}_{\text{hai}} - \boldsymbol{T}_{el}{}^{l}\dot{\tilde{\boldsymbol{\omega}}}_l{}^{l}\boldsymbol{R}_{\text{lai}} = \boldsymbol{T}_{eh}{}^{h}\boldsymbol{a}_h - \boldsymbol{T}_{el}{}^{l}\boldsymbol{a}_l - \boldsymbol{T}_{eh}\tilde{\boldsymbol{R}}_{\text{hai}}{}^{h}\boldsymbol{\alpha}_h \\ &+ \boldsymbol{T}_{el}\tilde{\boldsymbol{R}}_{\text{lai}}{}^{l}\boldsymbol{\alpha}_l + \boldsymbol{T}_{eh}{}^{h}\tilde{\boldsymbol{\omega}}_h{}^{h}\tilde{\boldsymbol{\omega}}_h{}^{h}\boldsymbol{R}_{\text{hai}} - \boldsymbol{T}_{el}{}^{l}\tilde{\boldsymbol{\omega}}_l{}^{l}\tilde{\boldsymbol{\omega}}_l{}^{l}\boldsymbol{R}_{\text{lai}} \\ &+ \boldsymbol{T}_{eh}\tilde{\boldsymbol{R}}_{\text{hai}}\boldsymbol{I}_h^{-1h}\tilde{\boldsymbol{\omega}}_h\boldsymbol{I}_h{}^{h}\boldsymbol{\omega}_h - \boldsymbol{T}_{el}\tilde{\boldsymbol{R}}_{\text{lai}}\boldsymbol{I}_h^{-1l}\tilde{\boldsymbol{\omega}}_l{}^{l}\boldsymbol{\omega}_l \end{aligned} \tag{21}$$

using Eqs. (7) and (8).

B. Rigid-Body Model

To identify $\boldsymbol{A}$ and $\boldsymbol{b}$, Eqs. (20) and (21) are substituted into Eq. (16), which is rearranged as

$$\ddot{g}_i = 2\boldsymbol{L}_i^T\left(\boldsymbol{T}_{eh}{}^{h}\boldsymbol{a}_h + \boldsymbol{T}_{eh}\tilde{\boldsymbol{R}}_{\text{hai}}{}^{h}\boldsymbol{\alpha}_h - \boldsymbol{T}_{el}{}^{l}\boldsymbol{a}_l - \boldsymbol{T}_{el}\tilde{\boldsymbol{R}}_{\text{lai}}{}^{l}\boldsymbol{\alpha}_l\right) - b_i \tag{22}$$

$\boldsymbol{A}_i$ can thus be identified as

$$\boldsymbol{A}_i = 2\boldsymbol{L}_i^T\begin{bmatrix}\boldsymbol{T}_{eh} & \boldsymbol{T}_{eh}\tilde{\boldsymbol{R}}_{\text{hai}} & -\boldsymbol{T}_{el} & -\boldsymbol{T}_{el}\tilde{\boldsymbol{R}}_{\text{lai}}\end{bmatrix}_{3\times 12} \tag{23}$$

and b_i as

$$\begin{aligned}b_i = &-2\dot{\boldsymbol{L}}_i^T\dot{\boldsymbol{L}}_i - 2\boldsymbol{L}_i^T\Big(\boldsymbol{T}_{eh}{}^{h}\tilde{\boldsymbol{\omega}}_h{}^{h}\tilde{\boldsymbol{\omega}}_h{}^{h}\boldsymbol{R}_{\text{hai}} - \boldsymbol{T}_{el}{}^{l}\tilde{\boldsymbol{\omega}}_l{}^{l}\tilde{\boldsymbol{\omega}}_l{}^{l}\boldsymbol{R}_{\text{lai}} \\ &+ \boldsymbol{T}_{eh}\tilde{\boldsymbol{R}}_{\text{hai}}\boldsymbol{I}_h^{-1h}\tilde{\boldsymbol{\omega}}_h\boldsymbol{I}_h{}^{h}\boldsymbol{\omega}_h - \boldsymbol{T}_{el}\tilde{\boldsymbol{R}}_{\text{lai}}\boldsymbol{I}_h^{-1l}\tilde{\boldsymbol{\omega}}_l\boldsymbol{I}_l{}^{l}\boldsymbol{\omega}_l\Big)\end{aligned} \tag{24}$$

Finally, the full constraint equation of Eq. (3) can be found

$$\boldsymbol{A} = \begin{bmatrix}\boldsymbol{A}_1 \\ \boldsymbol{A}_2 \\ \vdots \\ \boldsymbol{A}_m\end{bmatrix}_{m\times 12} \qquad \boldsymbol{b} = \begin{bmatrix}b_1 \\ b_2 \\ \vdots \\ b_m\end{bmatrix}_{m\times 1} \qquad \ddot{\boldsymbol{q}}_u = \begin{bmatrix}{}^{h}\boldsymbol{a}_h \\ {}^{h}\boldsymbol{\alpha}_h \\ {}^{l}\boldsymbol{a}_l \\ {}^{l}\boldsymbol{\alpha}_l\end{bmatrix}_{12\times 1} \tag{25}$$

which can then be inserted into Eq. (6) to yield $\ddot{\boldsymbol{q}}$. Using this expression in Eqs. (7–10), the final model is achieved.

Note that, for a suspension type with only a single attachment point on the helicopter, the model will show no coupling between the yaw motion of the helicopter and the load. This is not an entirely correct representation, as there is a small coupling present from the twisting wire. However, this is simply modeled as a small spring between the yaw angle of the helicopter and the load.

IV. Wire Slackening and Tightening

Wire slackening and tightening is a subject that has not been researched much in the literature. This is mainly due to the fact that the slackening and tightening of wires are situations that should generally be avoided with a slung load. However, there are two good reasons for incorporating slackening and tightening into the model. First, it is desirable to avoid wire slackening during flight, and thus it is necessary to be able to determine when the phenomenon occurs. Second, during takeoff and landing, tightening and slackening of wires are unavoidable. In the following, a simple way of incorporating the ability to handle wire slackening and tightening into the model will be discussed. The situations with a slack and a taut wire are illustrated in Fig. 3.

A. Wire Slackening and Tightening Detection

Slackening of wires can be determined by projecting the generalized constraint forces onto the wires and determining if the forces acting on the wires are tensioning or compressing. This is done by first finding the total constraint force acting in the attachment point, given by $\boldsymbol{Q}_c$. This is then transformed into the Earth-fixed frame and projected onto a unit wire vector, which yields

$$Q_{bwi} = \boldsymbol{N}_i^T[\boldsymbol{T}_{eb}(\tilde{\boldsymbol{\tau}}_{bc}\boldsymbol{R}_{\text{bai}} + \boldsymbol{F}_{bc})] \tag{26}$$

where Q_{bwi} is the constraint force acting on the ith wire from body b and $\boldsymbol{N}_i \in \mathbb{R}^3$ is a unit vector along $\boldsymbol{L}_i \in \mathbb{R}^3$. The constraint forces and torques for body b, given by $\boldsymbol{Q}_c$, are denoted by $\boldsymbol{F}_{bc}$ and $\boldsymbol{\tau}_{bc}$. The two contributions from the helicopter and the load are then subtracted as $Q_{wi} = Q_{hwi} - Q_{lwi}$, which makes it possible to determine if the resulting constraint forces acting on the wire are compressing (negative) or tensioning (positive).

A tightening of a wire can be determined by observing the norm of the wire; when it becomes equal to or larger than the nominal length of the wire, a tightening has occurred. This means that, when the distance between the attachment points on the helicopter and the load becomes equal to or longer than the actual wire length, the wire becomes taut. The slackening and tightening state machine is shown in Fig. 4.

B. Wire Slackening and Tightening Response

Handling the response of a wire slackening is quite simple, whereas a tightening response is somewhat more complicated. When a slackening has been determined for wire i, this wire is removed from the constraint equation by setting $\boldsymbol{A}_i = \boldsymbol{0}$ and $b_i = 0$.

Any tightening (both elastic and inelastic) can be modeled using conservation of momentum. The relationship between translational and angular velocity before and after the impact can be described in the following way, using the standard relationship between linear

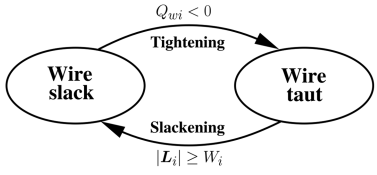

Fig. 4 State machine for the wire slackening and tightening mechanism.

and angular momentum given by the impulse J of the tightening

$$ {}^{h}_{2}\boldsymbol{v}_h = {}^{h}_{1}\boldsymbol{v}_h + m_h^{-1\,h}\boldsymbol{N}_i J \tag{27} $$

$$ {}^{l}_{2}\boldsymbol{v}_l = {}^{l}_{1}\boldsymbol{v}_l - m_l^{-1\,l}\boldsymbol{N}_i J \tag{28} $$

$$ {}^{h}_{2}\boldsymbol{\omega}_h = {}^{h}_{1}\boldsymbol{\omega}_h + \boldsymbol{I}_h^{-1}(\tilde{\boldsymbol{R}}_{\text{hai}}{}^{h}\boldsymbol{N}_i J) \tag{29} $$

$$ {}^{l}_{2}\boldsymbol{\omega}_l = {}^{l}_{1}\boldsymbol{\omega}_l - \boldsymbol{I}_l^{-1}(\tilde{\boldsymbol{R}}_{\text{lai}}{}^{l}\boldsymbol{N}_i J) \tag{30} $$

where the situation just before and just after the tightening are denoted with presubscript ${}_1(\cdot)$ and ${}_2(\cdot)$, respectively.

A perfectly inelastic tightening is characterized by the relative velocity between the two attachment points projected onto the wire $({}^{e}\boldsymbol{v}_{\Delta}^{T}\,{}^{e}\boldsymbol{N}_i)$ being zero after the tightening. An elastic tightening is characterized by energy conservation, thus allowing the affected objects to bounce. Thus, a tightening can be described by

$$ -K_e\,{}^{e}\boldsymbol{N}_i^{T}\,{}^{e}_{1}\boldsymbol{v}_{\Delta} = {}^{e}\boldsymbol{N}_i^{T}\,{}^{e}_{2}\boldsymbol{v}_{\Delta} $$

where the elasticity in a tightening is described by a constant K_e. When $K_e = 0$, it describes an inelastic tightening, when $K_e = 1$ it describes an elastic tightening, and when $0 < K_e < 1$, it describes a combination of the two.

The relative velocity of the two attachment points can be described by the translational and angular velocity of the two bodies

$$ -K_e\,{}^{e}\boldsymbol{N}_i^{T}\,{}^{e}_{1}\boldsymbol{v}_{\Delta} = {}^{e}\boldsymbol{N}_i^{T}\left[\boldsymbol{T}_{eh}\left({}^{h}_{2}\boldsymbol{v}_h + {}^{h}_{2}\tilde{\boldsymbol{\omega}}_h\boldsymbol{R}_{\text{hai}}\right) - \boldsymbol{T}_{el}\left({}^{l}_{2}\boldsymbol{v}_l + {}^{l}_{2}\tilde{\boldsymbol{\omega}}_l\boldsymbol{R}_{\text{lai}}\right)\right] \tag{31} $$

It is now possible to substitute the relations between the velocities before and after tightening, Eqs. (27–30) into Eq. (31), such that the equation only depends on velocities before the tightening and the impulse can be isolated

$$ J = \frac{-(1+K_e)\,{}^{e}\boldsymbol{N}_i^{T}\,{}^{e}_{1}\boldsymbol{v}_{\Delta}}{(1/m_h) + (1/m_l) - {}^{e}\boldsymbol{N}_i^{T}(\boldsymbol{T}_{eh}\tilde{\boldsymbol{R}}_{\text{hai}}\boldsymbol{I}_h^{-1}\tilde{\boldsymbol{R}}_{\text{hai}}{}^{h}\boldsymbol{N}_i + \boldsymbol{T}_{el}\tilde{\boldsymbol{R}}_{\text{lai}}\boldsymbol{I}_l^{-1}\tilde{\boldsymbol{R}}_{\text{lai}}{}^{l}\boldsymbol{N}_i)J} \tag{32} $$

By using Eq. (32) to determine the resulting impulse from the tightening and using this in Eqs. (27–30), it is possible to determine the tightening response for a wire.

V. Multilift Systems

Multilift systems (where two or more helicopters are used to lift the load) are of both theoretical and practical interest. From a practical point of view, there are many situations where there is an advantage in using two smaller helicopters to lift a load rather than one large one. From a theoretical point of view, the challenge of modeling and controlling multilift systems have been the focus of quite a bit of research during the past decades [5,16]. Multilift systems are traditionally considered highly complex systems and often result in correspondingly complex models. Fortunately, the modeling approach introduced in this paper can easily be extended to general multilift systems simply by augmenting the equations with extra bodies. It should be noted that, although the general equations derived in this section cover l wires for each helicopter and k helicopters, almost all practical multilift systems use only one wire for each helicopter, that is, $l = k$.

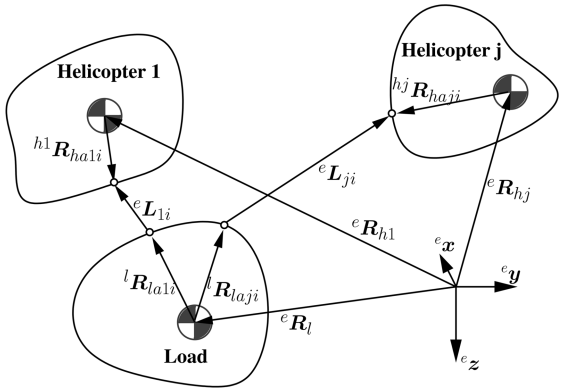

Fig. 5 Configuration of a multilift system with two helicopters shown with the first and the *j*th helicopter.

In the following, the focus will be on point-to-point dual-lift suspension systems, like the dual pendant suspension and the straight dual-lift suspension, although, systems including spreader bars can easily be modeled by including the bar as an extra body using the methods presented. A general point-to-point multilift suspension system is shown in Fig. 5.

To describe the system shown in Fig. 5, the equations derived previously are simply augmented with the new body in the system:

$$ \boldsymbol{q} = \begin{bmatrix} \boldsymbol{R}_{h1} \\ \boldsymbol{\theta}_{h1} \\ \vdots \\ \boldsymbol{R}_{hk} \\ \boldsymbol{\theta}_{hk} \\ \boldsymbol{R}_{l} \\ \boldsymbol{\theta}_{l} \end{bmatrix}_{n\times 1} \qquad \ddot{\boldsymbol{q}}_u = \begin{bmatrix} {}^{h1}\boldsymbol{a}_{h1} \\ {}^{h1}\boldsymbol{\alpha}_{h1} \\ \vdots \\ {}^{hk}\boldsymbol{a}_{hk} \\ {}^{hk}\boldsymbol{\alpha}_{hk} \\ {}^{l}\boldsymbol{a}_{l} \\ {}^{l}\boldsymbol{\alpha}_{l} \end{bmatrix}_{n\times 1} \tag{33} $$

The constraint Eq. (16) can then be reformulated to encompass multiple bodies such that the constraint equation describes the ith wire on the jth body. $\boldsymbol{A}$ and $\boldsymbol{b}$ then become

$$ b_{ji} = -2\dot{\boldsymbol{L}}_{ij}^{T}\dot{\boldsymbol{L}}_{ij} - 2\boldsymbol{L}_{ij}^{T}(\boldsymbol{T}_{ehj}{}^{hj}\tilde{\boldsymbol{\omega}}_{hj}{}^{hj}\tilde{\boldsymbol{\omega}}_{hj}\boldsymbol{R}_{haji} - \boldsymbol{T}_{el}{}^{l}\tilde{\boldsymbol{\omega}}_{l}{}^{l}\tilde{\boldsymbol{\omega}}_{l}\boldsymbol{R}_{laji} + \boldsymbol{T}_{ehj}\tilde{\boldsymbol{R}}_{haji}\boldsymbol{I}_{hj}^{-1\,hj}\tilde{\boldsymbol{\omega}}_{hj}\boldsymbol{I}_{hj}{}^{hj}\boldsymbol{\omega}_{hj} - \boldsymbol{T}_{el}\tilde{\boldsymbol{R}}_{laji}\boldsymbol{I}_{l}^{-1\,l}\tilde{\boldsymbol{\omega}}_{l}\boldsymbol{I}_{l}{}^{l}\boldsymbol{\omega}_{l}) $$

$$ \boldsymbol{A}_{ji} = 2\boldsymbol{L}_{ji}^{T}\begin{bmatrix} \boldsymbol{0}_{3\times nj} & \boldsymbol{T}_{ehj} & \boldsymbol{T}_{ehj}\tilde{\boldsymbol{R}}_{haji} & \boldsymbol{0}_{3\times n(k-j-1)} & \boldsymbol{0}_{3\times nk} & -\boldsymbol{T}_{el} & -\boldsymbol{T}_{el}\tilde{\boldsymbol{R}}_{laji} \end{bmatrix} $$

$$\boldsymbol{A} = \begin{bmatrix} \boldsymbol{A}_{11} \\ \boldsymbol{A}_{12} \\ \vdots \\ \boldsymbol{A}_{ji} \\ \vdots \\ \boldsymbol{A}_{kl} \end{bmatrix}_{kl\times n} \qquad \boldsymbol{b} = \begin{bmatrix} b_{11} \\ b_{12} \\ \vdots \\ b_{ji} \\ \vdots \\ b_{kl} \end{bmatrix}_{kl\times 1}$$

where the jith component of $\boldsymbol{b}$ is equal to the single helicopter case and where the jith block of $\boldsymbol{A}$ has zeros on the rows not related to the jth body.

If the equations for single-lift and multilift systems are compared, it is clear that the process of augmenting the slung-load model with additional bodies is indeed simple.

VI. Rotor Downwash Effects on Load

The modeling of the interaction between load and main rotor wake is done using [4] as inspiration. The wake is modeled using two elliptical cylinders, one to describe the near wake and one for the far wake. It is assumed that the load is situated far enough downstream to be in the far wake, and therefore the region between the near and far wake is not considered here. The direction of the wake near the rotor is given by the wake-skew angle

$$\chi_w = \arctan\left(\frac{-\lambda_{mr}}{\mu_{mr}}\right) \tag{34}$$

where $\mu_{mr} = \sqrt{\mu_x^2 + \mu_y^2 + \mu_z^2}$. This angle changes further down the wake as the inflow velocity changes. Classical momentum theory predicts a change from v_w at the rotor to $2v_w$ in the fully developed wake when the inflow is assumed uniform and swirl components are neglected. Given this, a prediction of the wake centerline can be made. It is assumed that the distance from the rotor to the far wake can be described as $1.5R_{mr}$ [4,17]. In the near wake, the cylinder is centered around the velocity vector ${}^h\boldsymbol{V}'$

$${}^h\boldsymbol{V}' = {}^h\boldsymbol{v}_w - {}^h\boldsymbol{V} \tag{35}$$

where ${}^h\boldsymbol{V}_w$ is a vector perpendicular to the tip path plane with the length v_w. In the far field, the wake is centered around

$${}^h\boldsymbol{V}'' = 2{}^h\boldsymbol{v}_w - {}^h\boldsymbol{V} \tag{36}$$

The position of the far wake starting point is described by the vector $\boldsymbol{R}_{\text{fw}}$, which is then given by

$${}^h\boldsymbol{R}_{\text{fw}} = 1.5R_{mr}\frac{{}^h\boldsymbol{V}'}{|{}^h\boldsymbol{V}'|} \tag{37}$$

as illustrated in Fig. 6.

To calculate the boundaries of the far wake, we use the fact that the wake has a circular cross section at the tip path plane. This means that the cross section perpendicular to ${}^h\boldsymbol{V}'$ is an ellipse with a major and minor axis radius of

$$R'_{\text{ma}} = R_{mr}, \qquad R'_{\text{mi}} = R_{mr}\cos(\chi_s) \tag{38}$$

If we assume that the tube contracts equally along both axes, the cross section ellipse perpendicular to ${}^h\boldsymbol{V}''$ in the far wake can be described by

$$R''_{\text{ma}} = K_{\text{con}}R'_{\text{ma}}, \qquad R''_{\text{mi}} = K_{\text{con}}R'_{\text{mi}} \tag{39}$$

where $K_{\text{con}} \in [0; 1]$ is the contraction factor.

The continuity equation used in the momentum theory states that the mass flow is constant throughout the wake and, if we assume constant pressure both in the near and far wake, the equation is only dependent on the tube cross section area and velocity. This means that the contraction of the tube can be calculated as

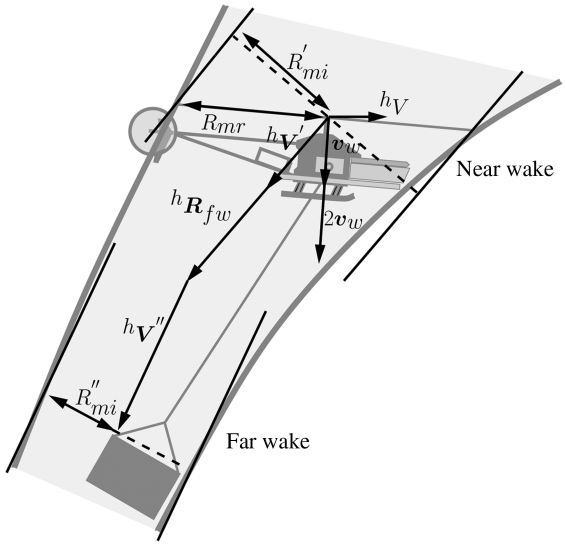

Fig. 6 Rotor wake geometry.

$$\pi R'_{\text{ma}}R'_{\text{mi}}\|{}^h\mathbf{V}'\| = \pi R''_{\text{ma}}R''_{\text{mi}}\|{}^h\mathbf{V}''\| \Leftrightarrow R'_{\text{ma}}R'_{\text{mi}}\|{}^h\boldsymbol{V}'\|$$
$$= K_{\text{con}}R'_{\text{ma}}K_{\text{con}}R'_{\text{mi}}\|{}^h\boldsymbol{V}''\| \Leftrightarrow K_{\text{con}} = \sqrt{\frac{\|{}^h\boldsymbol{V}'\|}{\|{}^h\boldsymbol{V}''\|}} \tag{40}$$

A. Load Wake Interaction

The position of the load relative to the beginning of the far wake can be calculated as

$${}^h\boldsymbol{R}_{\text{wl}} = \boldsymbol{T}_{he}({}^e\boldsymbol{R}_l - {}^h\boldsymbol{R}_h) - {}^h\boldsymbol{R}_{\text{fw}} \Leftrightarrow {}^h\boldsymbol{R}_{\text{wl}} = {}^h\boldsymbol{R}_{Rl} - {}^h\boldsymbol{R}_{\text{fw}} \tag{41}$$

in the helicopter fixed frame. We now introduce a frame which is fixed in the wake such that the z axis points along $\boldsymbol{V}''$ and the x axis points in the opposite direction of $\boldsymbol{V}$. The Euler angles for the transformation between the wake frame and the helicopter frame are then determined as

$$\phi_w = 0, \qquad \theta_w = \arccos\left(\frac{\sqrt{v_x^2 + v_y^2}}{\sqrt{(2v_w - v_z)^2 + v_x^2 + v_y^2}}\right)$$
$$\psi_w = \arccos\left(\frac{v_x}{\sqrt{v_x^2 + v_y^2}}\right)$$

This can be used to transform the position of the load relative to the wake into the frame

$${}^w\boldsymbol{R}_{\text{wl}} = \boldsymbol{T}_{\text{wh}}{}^h\boldsymbol{R}_{\text{wl}} \tag{42}$$

which makes it possible to compare it directly to the wake boundaries found earlier. Using this, the load is then assumed to be inside the wake when the following condition is true

$$\left(\frac{x_{\text{wl}}}{R''_{\text{mi}}}\right)^2 + \left(\frac{y_{\text{wl}}}{R''_{\text{ma}}}\right)^2 < 1 \tag{43}$$

and outside when false (under the assumption that the load is more than $1.5R_{mr}$ under the helicopter). The preceding can be evaluated by substituting in Eqs. (38) and (39)

$$\left(\frac{x_{\text{wl}}}{K_{\text{con}}R_{mr}\cos(\chi_s)}\right)^2 + \left(\frac{y_{\text{wl}}}{K_{\text{con}}R_{mr}}\right)^2 < 1 \tag{44}$$

When the load is inside the wake, the load velocities are augmented with the following term

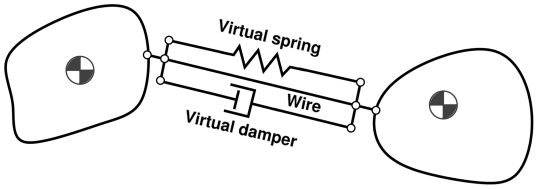

Fig. 7 Numerical correction of constraints by inserting a virtual spring and damper system along the wires. This ensures that integration errors do not result in an unbounded constraint error.

$$^{l}\boldsymbol{V}_{\mathrm{wl}} = \boldsymbol{T}_{le}\boldsymbol{T}_{eh} = \begin{bmatrix} 0 \\ 0 \\ 2v_w \end{bmatrix} \tag{45}$$

which can then be used to calculate the drag on the load. When outside the wake, only the load velocities are used.

B. Load Aerodynamics

The aerodynamics of the load is highly dependent on the type and shape of the actual object suspended. In this case, we choose to use a simple drag-based model, but this can of course be exchanged with more advanced models for specific objects. The drag forces are defined along the body coordinate system axis and are assumed to act in the body center of mass and thus cause no torques. They can be calculated using the standard quadratic drag function, which describes the drag as proportional to the speed squared

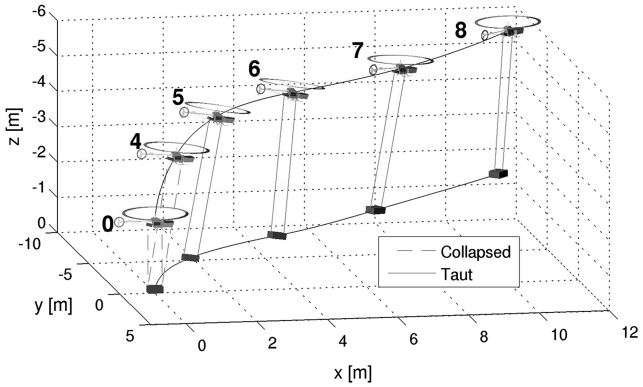

Fig. 8 Three-dimensional plot of the dual-wire takeoff example with time line (simulation).

$$^{l}F_{dl} = -0.5\rho \begin{bmatrix} \delta_{xl} D_{xl} |^{l}v_{xl}| {}^{l}v_{xl} \\ \delta_{yl} D_{yl} |^{l}v_{yl}| {}^{l}v_{yl} \\ \delta_{zl} D_{zl} |^{l}v_{zl}| {}^{l}v_{zl} \end{bmatrix} \tag{46}$$

where the load velocity $^{l}v_{l}$ includes the wake velocity of Eq. (45).

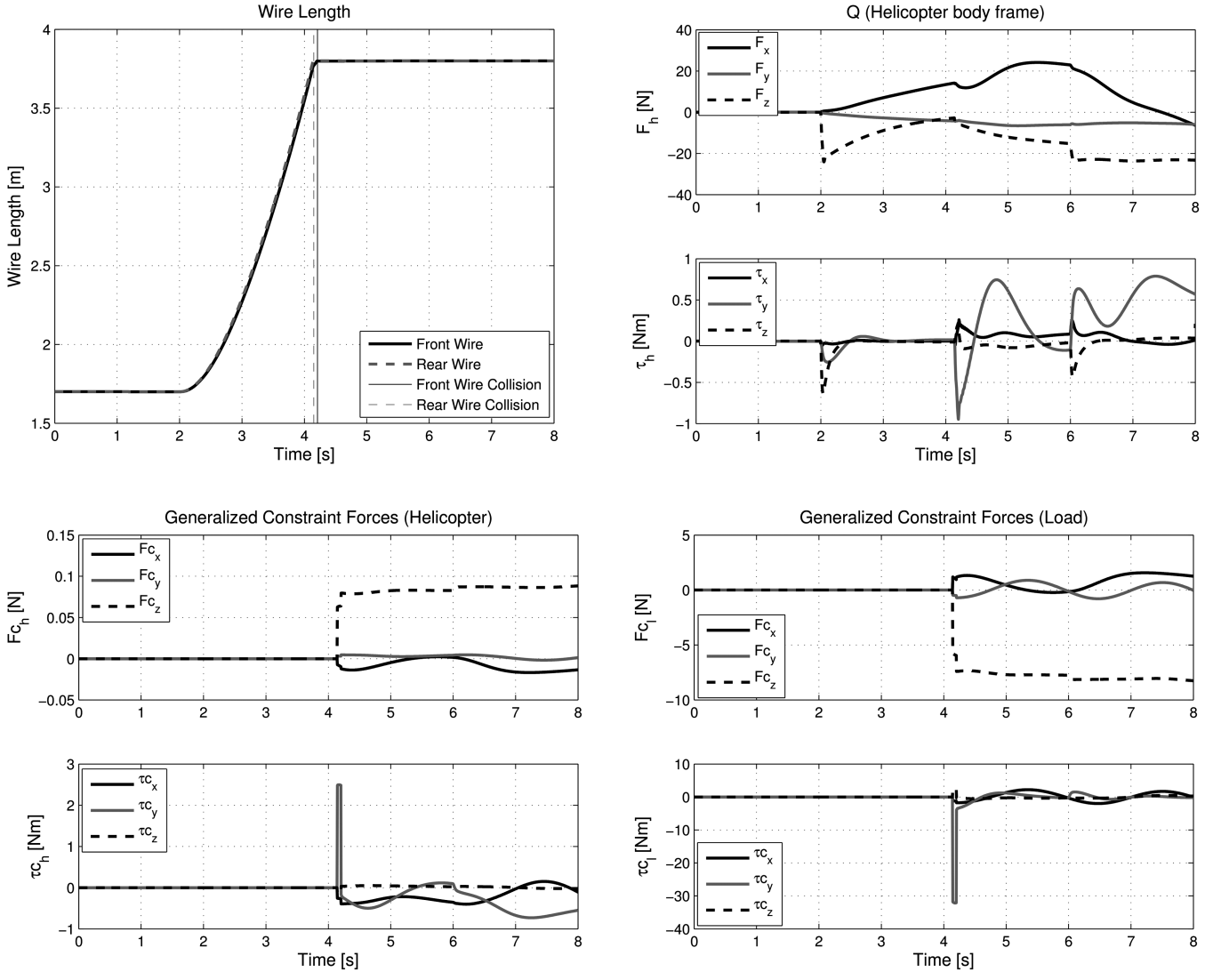

Fig. 9 Helicopter and load wire length and forces during dual-wire takeoff (simulation).

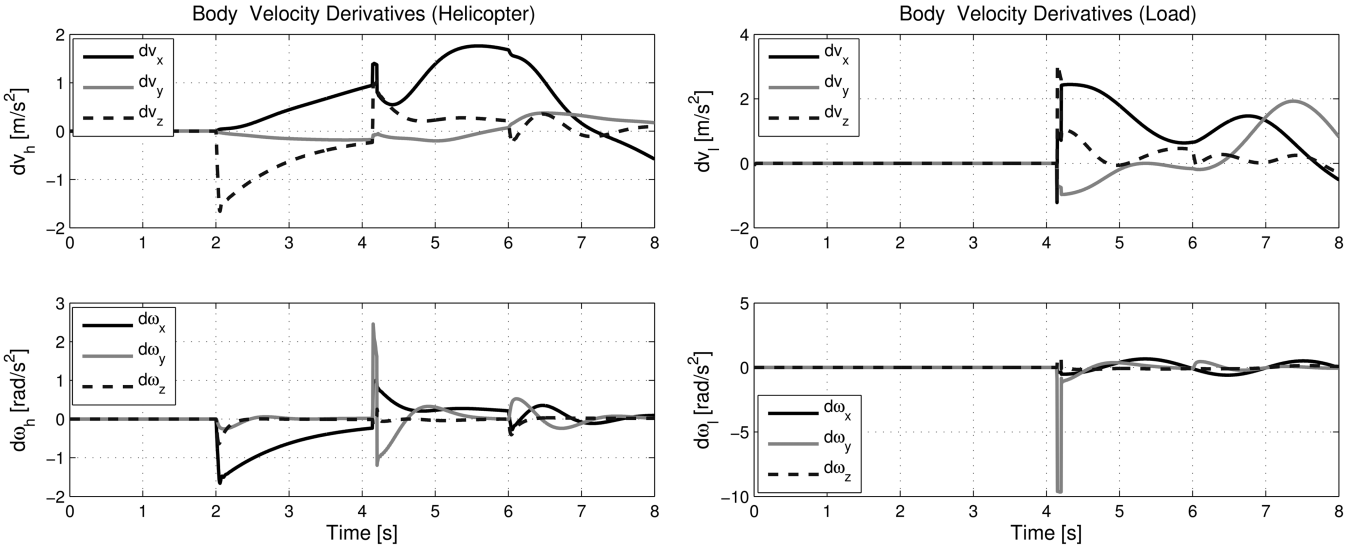

Fig. 10 Helicopter and load acceleration response during dual-wire takeoff.

VII. Numerical Considerations

One of the disadvantages of using a full-state model instead of a reduced-state model is that numerical integration errors will, over time, violate the constraints. This is due to the fact that the dynamic equations ensure that the system obeys the constraints in an acceleration sense, such that

$$\ddot{g}(\ddot{\boldsymbol{q}}_a, \ddot{\boldsymbol{q}}_b, \boldsymbol{q}) = 0 \tag{47}$$

in accordance with Eq. (3). There is no direct enforcement of the constraints in a velocity and position sense, and the error on the constraints can therefore grow unbounded. This means that the length of the wires will start to drift as the simulation progresses.

The severity of the problem is highly dependent on the chosen integration method and step size used in the integration. Furthermore, the problem can be lessened by using appropriate coordinates, which reduces the integration errors. In this case, the absolute position of the slung load could be exchanged with slung-load position relative to the helicopter, which would reduce, but not remove, the drift problem. It is a widely recognized problem in the literature [18] and several different approaches have been suggested to counter this problem; the most well known is the method suggested by Baumgarte [19]. However, a simpler alternative approach will be suggested here, conceived through a consideration of how the problem affects the system, using numerical feedback from the constraints in the dynamics equation.

From a physical point of view, the drifting constraint problem results in the length of the wires drifting. This means that, when the wire becomes too long, we should apply a force along it to pull it back into shape, and vice versa. A simple way of doing this is to introduce a small virtual spring-damper system in parallel with each wire, as shown in Fig. 7. The spring will then try to keep the wire length constant and thus introduce a penalty on the constraint error. The damper is necessary to reduce numerical oscillations.

It is important to note that the introduction of the virtual spring-damper system only exists in simulation, has no actual effect on the dynamics of the system, and does not make the wires elastic. It is simply introduced to ensure that integration errors do not result in drifting wire lengths in the simulation.

The spring force $\boldsymbol{F}_s$ and damper force $\boldsymbol{F}_d$ can be found using the constraint equation, and the time derivative of it, and projecting along the wires. This is done as

$$\boldsymbol{F}_{si} = k_s g_i(\boldsymbol{q}) \boldsymbol{N}_i \tag{48}$$

$$\boldsymbol{F}_{di} = -c_d \dot{g}_i(\boldsymbol{q}) \boldsymbol{N}_i \tag{49}$$

where k_s is the spring constant and c_d is the damper constant. The calculated forces can then be used to calculate the resulting accelerations which are appended to Eq. (6) as

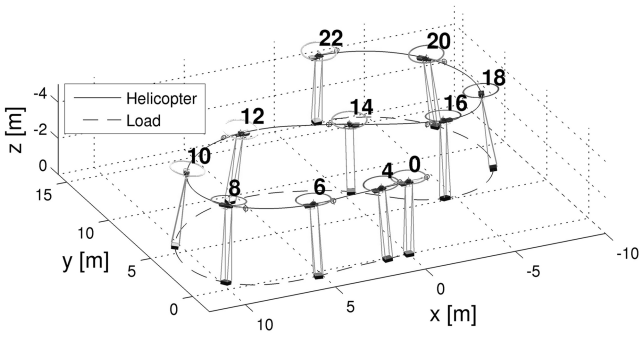

Fig. 11 Three-dimensional plot with time line of the helicopter and load with the inverted-V suspension system seen in perspective (simulation).

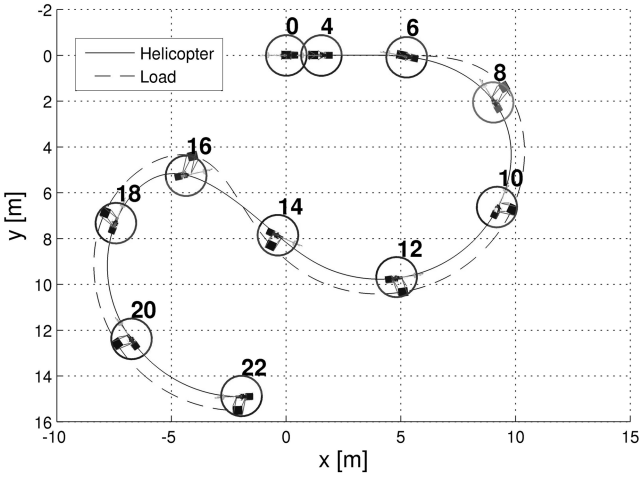

Fig. 12 Top view with time line of the helicopter and load with the inverted-V suspension system (simulation).

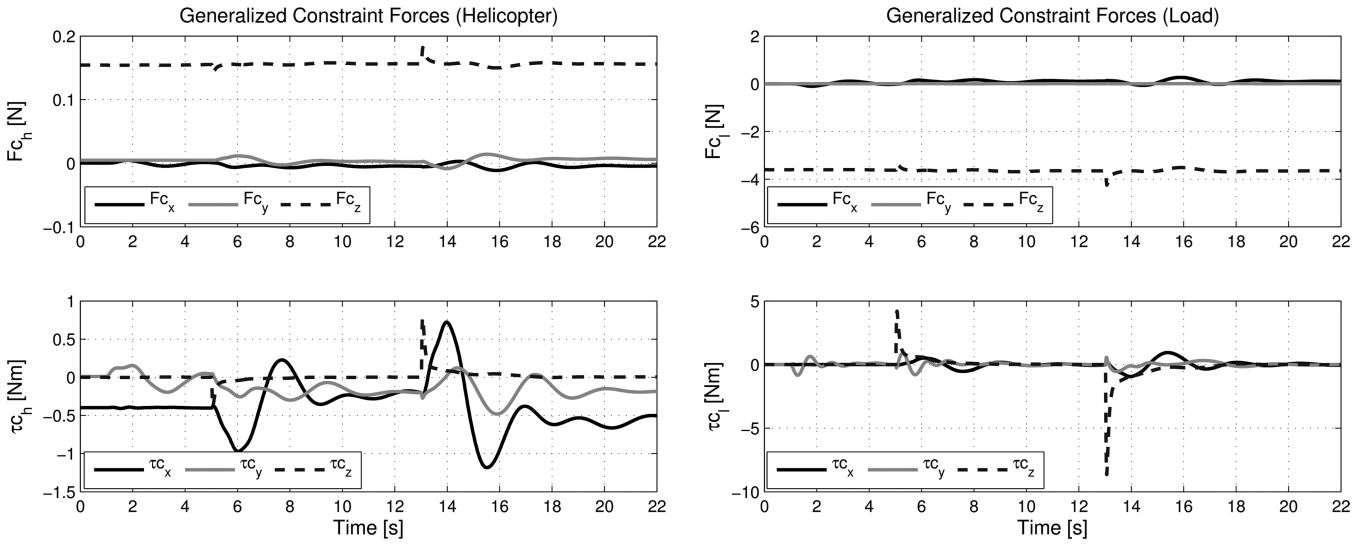

Fig. 13 Helicopter and load forces during S maneuver with an inverted-V suspension (simulation).

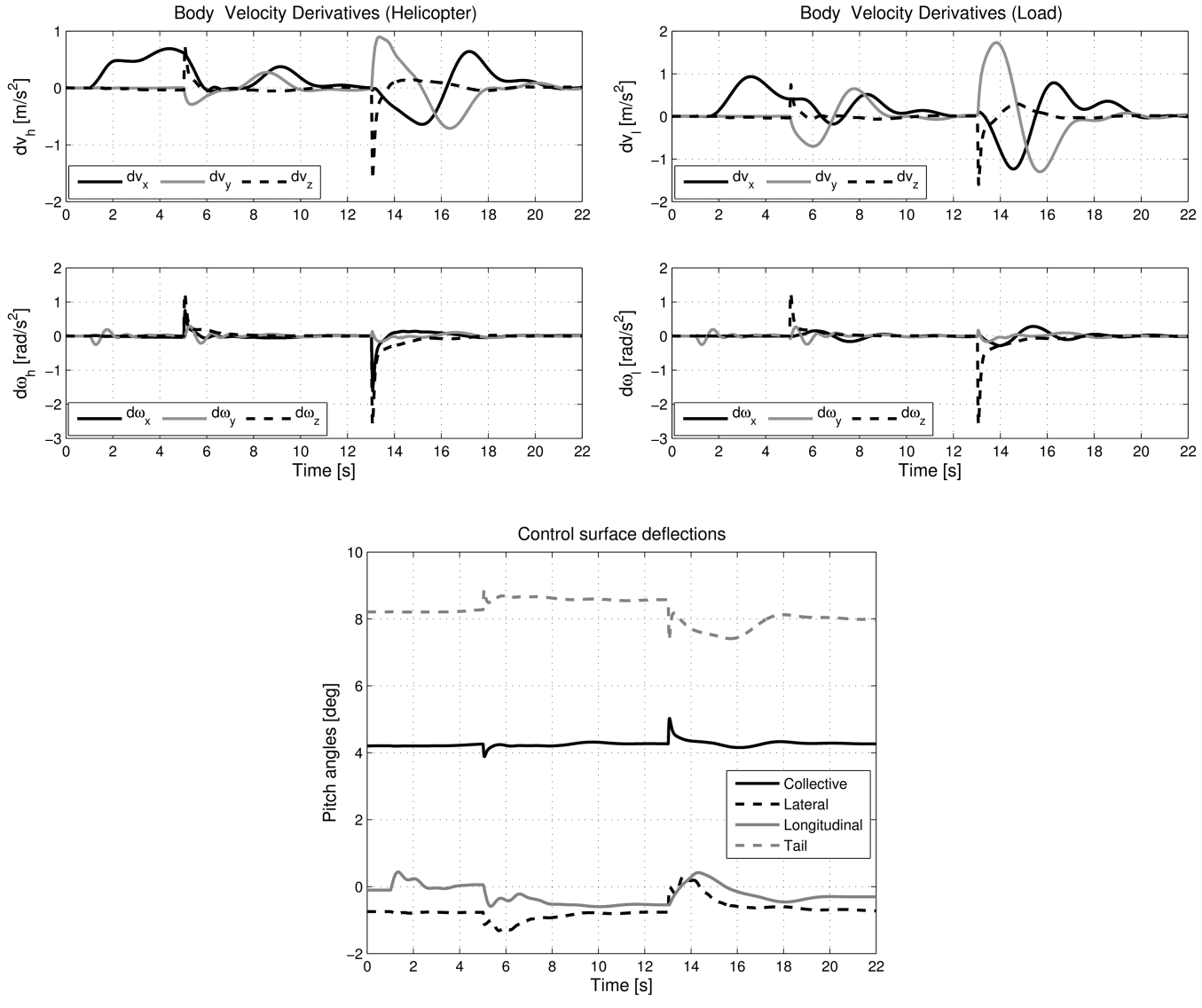

Fig. 14 Helicopter and load acceleration response and control input during S maneuver with an inverted-V suspension (simulation).

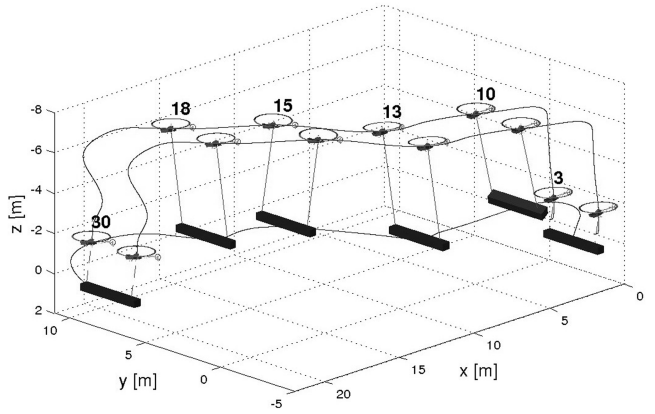

Fig. 15 Three-dimensional plot with time line of the helicopters and load in a dual-lift configuration seen in perspective (simulation).

$$\ddot{\boldsymbol{q}} = \boldsymbol{a} + \boldsymbol{M}^{-1/2}(\boldsymbol{A}\boldsymbol{M}^{-1/2})^{+}(\boldsymbol{b} - \boldsymbol{A}\boldsymbol{a}) + \begin{bmatrix} m_h^{-1}\sum_{i=1}^{m} \boldsymbol{T}_{he}(\boldsymbol{F}_{si} + \boldsymbol{F}_{di}) \\ \boldsymbol{I}_h^{-1}\sum_{i=1}^{m} \tilde{\boldsymbol{R}}_{\mathrm{hai}}\boldsymbol{T}_{he}(\boldsymbol{F}_{si} + \boldsymbol{F}_{di}) \\ m_l^{-1}\sum_{i=1}^{m} \boldsymbol{T}_{le}(\boldsymbol{F}_{si} + \boldsymbol{F}_{di}) \\ \boldsymbol{I}_l^{-1}\sum_{i=1}^{m} \tilde{\boldsymbol{R}}_{\mathrm{hai}}\boldsymbol{T}_{le}(\boldsymbol{F}_{si} + \boldsymbol{F}_{di}) \end{bmatrix}_{12\times 1} \tag{50}$$

VIII. Simulation

A number of different simulation scenarios are presented here to illustrate the functionality of the model. An 18-state helicopter model (not including rigid-body equations) is used together with the slung-load model. The helicopter model includes second-order actuator dynamics with saturation, blade element theory for main and tail rotor forces and torques, flapping dynamics for main rotor and stabilizer bar, and momentum theory for the inflow model [20,21].

Simulations are performed using MATLAB/Simulink with the model implemented as *C* code in *S* functions. Integration is done using fourth-order Runge–Kutta with a fixed step size of 0.005 s and the simulation runs faster than real time on a 2 GHz Pentium 4.

A. Dual-Wire Takeoff Example

To illustrate the modeling of the wire slackening and tightening phenomena, a takeoff situation is simulated using a dual-wire suspension. The helicopter is started in hover, 2 m above the 1.5 kg load, which is on the ground. The length of the wires is set to 3.8 m, which means that they start out slack. A positive collective pitch and forward cyclic pitch step is then applied to the helicopter, which starts to move forward and upward. At time 4.15 and 4.25 s, the two wires become taut and the load is lifted off the ground, as shown in Fig. 8.

The rear wire tightens first due to the pitching of the helicopter, as can be seen from the wire length plot in Fig. 9. It shows the direct distance between the attachment points and when the distance

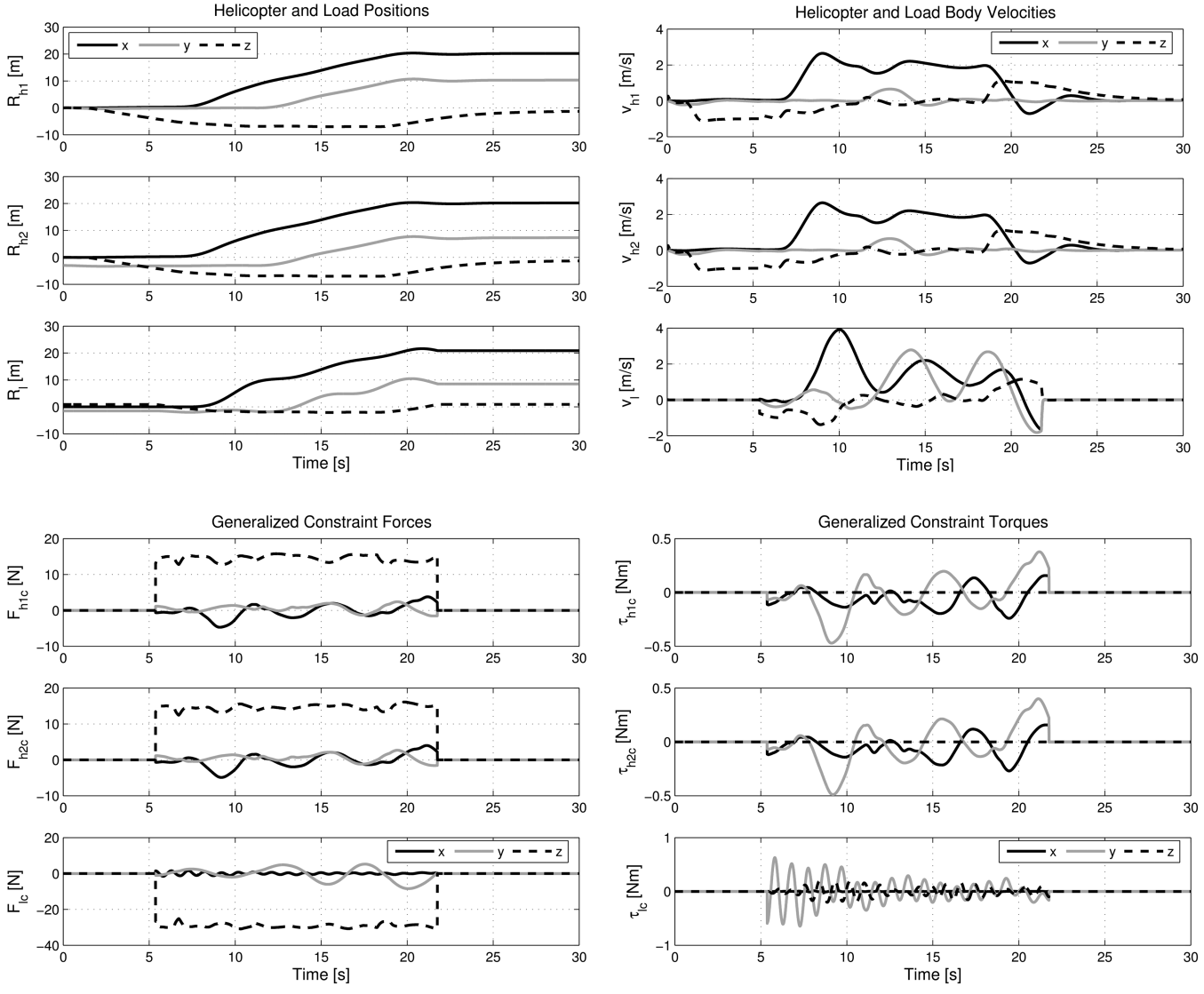

Fig. 16 Helicopter and load response in dual-lift configuration (simulation).

becomes equal to the taut wire length. The result from this tightening is clear from the body acceleration plots in Fig. 10, where it can be seen that the tightening results in a backward pitching (positive) and downward motion for the helicopter, as well as a forward pitching (negative) and upward motion for the load. Shortly after the second wire becomes taut, the pitching motions of the load and the helicopter become aligned, and the load is lifted off the ground.

As the helicopter starts in a trimmed hover state, it is initially not affected by any resulting force, which can be seen from the generalized applied forces plot in Fig. 9. From the generalized constraint force plot, it is clear that no constraint forces are present when the wires are slack. It can be seen that, when the first wire becomes taut, it results in a pitching torque as well as forces because the wire is off-center. However, shortly after, when the second wire becomes taut, this torque is canceled out.

B. Inverted-V Suspension Example

This example shows the helicopter performing an aggressive S maneuver with a four-wire inverted-V suspension with two attachment points on the helicopter. The mass of the load is 3 kg, the distance between the attachment points on both helicopter and load is 0.4 m, and wire length is 3.8 m. The maneuver is performed by applying a simple feedback controller to the system and the result is shown in Figs. 11 and 12.

The system starts from an initial trimmed hover and then performs first a tight left turn and then a tight right turn. It can be seen how the load swings out during the turns and drags a little behind the helicopter due to air drag. To visualize the behavior of the model, the graphs of Figs. 13 and 14 can be related to the modeling equations. The body velocity derivatives are given by Eqs. (7) and (8) and the generalized constraint forces are given by Eq. (5).

By observing Figs. 13 and 14, it can be seen that the system starts from hover where the thrust force generated by the helicopter must counter the gravity acting on the load. A commanded motion around $t = 1$ s with a longitudinal cyclic pitch change results in the helicopter tilting and moving forward. This helicopter motion changes the constraint forces to yield a forward torque on the load and a backward torque on the helicopter. The left turn is commanded at $t = 5$ s and the resulting right banking of the helicopter results in a counteracting negative constraint torque around the x axis, which changes to a positive torque when the load starts to swing out to the left relative to the helicopter. The opposite can be observed during the right turn at $t = 13$ s.

C. Twin-Lift Example

This example is used to illustrate how the model can be used for multilift systems. Two similar helicopters are used to lift a slung load with a mass of 5 m with the attachment points 3 m apart. The helicopters are independently controlled using linear feedback with each controller unaware of both the other helicopter and the load. The flight is shown in Fig. 15. The helicopters start in hover above the load and then pick up the load from the ground. They first fly 10 m forward, then execute a 45 deg right turn, fly 15 m forward, and finally set down the slung load on the ground.

In Fig. 16, the position and velocity are shown together with constraint forces and torques. It can be seen that the constraint forces are zero when the load is on the ground and the load oscillates underneath the helicopters. On the position plot, the distance between the helicopters can be seen.

IX. Flight Test Verification

Flight test verification of the model is presented in this section (see Fig. 17). The test setup is a modified 14 kg Bergen Industrial Twin equipped with appropriate sensors, such as a Novatel Global Positioning System, a HMR2300 magnetometer, a Falcon GX inertial measurement unit (IMU), and a camera used to determine the position of the load and yaw angle with respect to the helicopter. All the sensors are interfaced to the 1.8 GHz onboard laptop computer. The helicopter is capable of carrying slung loads of up to 4 kg and the load is equipped with an IMU as well as a laser range finder for tracking the contours of the ground.

The slung-load model is somewhat difficult to verify reliably compared to a helicopter stand-alone model. This is due to the fact that the helicopter's response to input changes is directly visible on the state vector without passing through long integrator chains. For instance, for the lateral cyclic pitch, the response is directly observable on the roll rate. When looking at the slung-load response, the input must pass through several rigid-body integrators before visibly affecting the slung-load motion. The direct input to the rigid-body model is a force vector. However, it is not possible to extract this force vector from the measurement data, and we are therefore limited to use the helicopter model as a force generator. For a lateral

Fig. 17 Aalborg University Bergen Industrial Twin flying with dual-wire demonstration slung load.

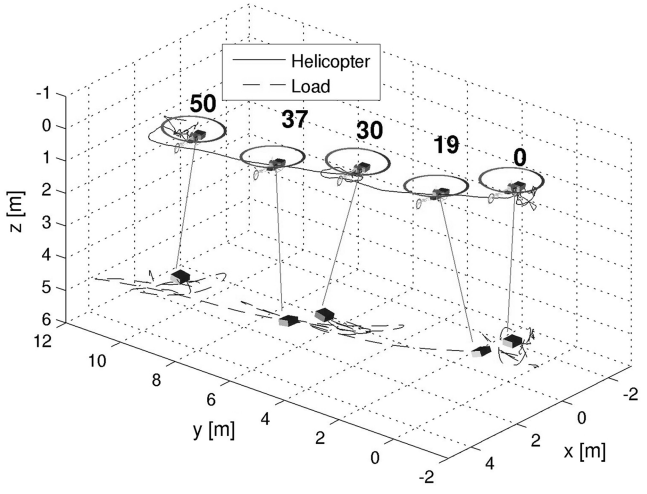

Fig. 18 Three-dimensional plot of the single-wire suspension system model verification test (with time line).

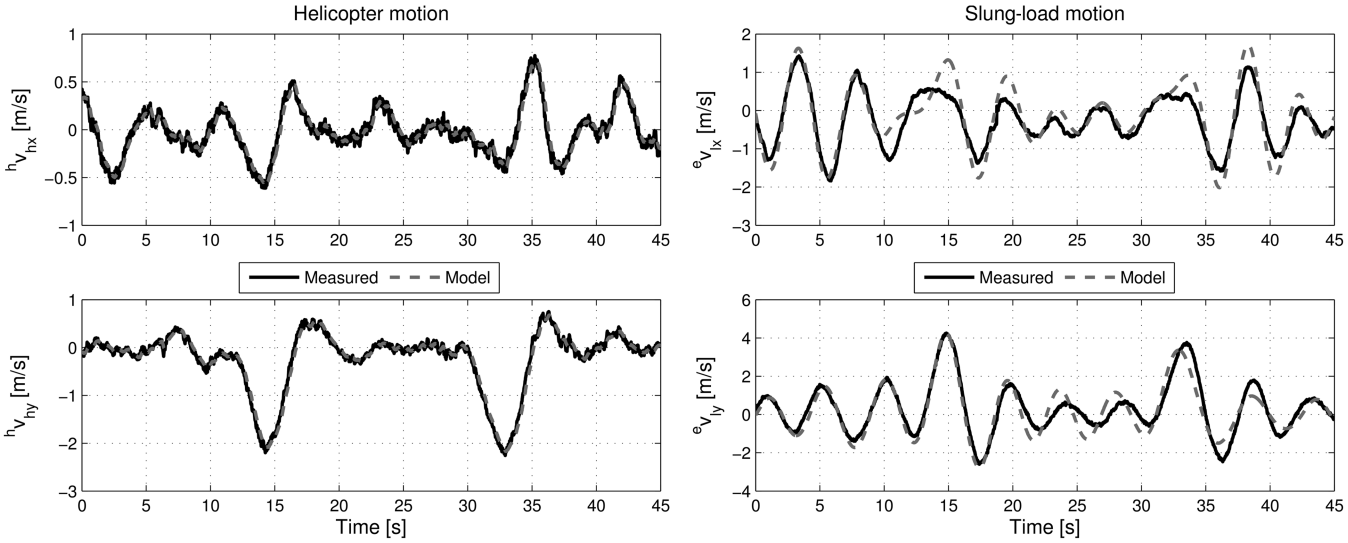

Fig. 19 Helicopter horizontal velocity model response (aided) vs measured response (left). Slung-load horizontal velocity model response vs measured response (right).

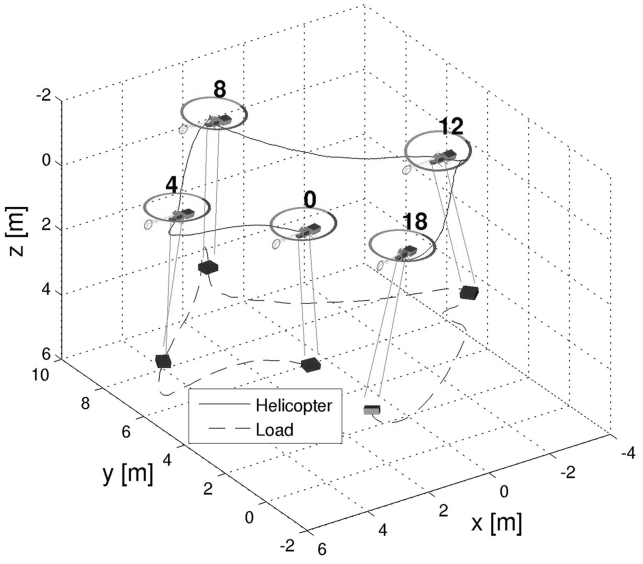

Fig. 20 Three-dimensional plot of dual-wire suspension system model verification test (with time line).

motion, the cyclic input becomes the helicopter roll rate, which integrates to helicopter roll. The helicopter attitude equates to a translational helicopter acceleration; this again equates to a slung-load acceleration which is integrated to velocity and position. Through this long integrator chain, small model errors and external wind disturbances can result in very large response discrepancies. It can therefore be difficult to assess whether the model provides a good description of the system.

To help reduce this problem, and for the slung-load model response to become more clear, we introduce a setup where the modeled helicopter position and Euler angles are forced to gradually converge to the estimated position and Euler angles. This means that the model is aided in following the absolute helicopter motion, whereas the slung load is allowed to move freely. In a sense, we create a force generator that, similar to the spring-damper approach presented in Sec. VII, continuously, but weakly, will attract the modeled helicopter position to the estimated position. We make sure that the model generates an almost correct unconstrained acceleration for the helicopter given by Eq. (6). This allows us to observe whether the slung-load model is capable of filling in the remaining elements of the model, which are the slung-load forces like gravity, drag, and, most importantly, the wire constraining forces.

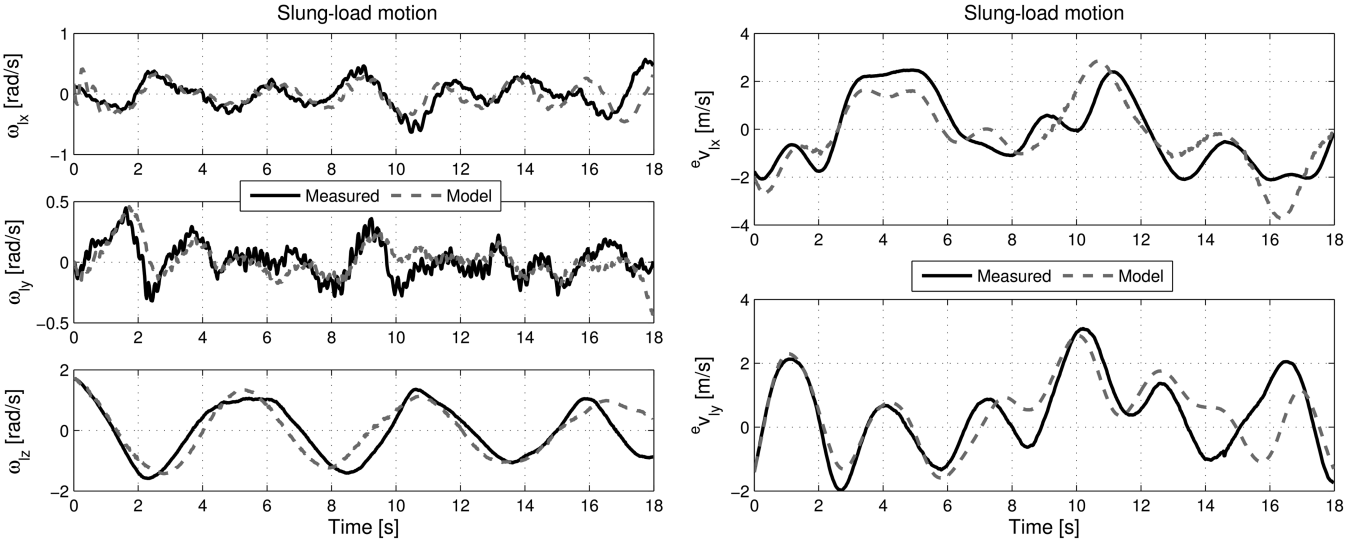

Fig. 21 Slung-load horizontal velocity model response vs measured response (left). Slung-load attitude rate response vs measured response (right).

A. Single-Wire Suspension System

In this test, we compare the responses of the model and the real system during two lateral steps with the single-wire suspension, as illustrated in Fig. 18. The test was performed using a controller in a closed loop on the helicopter motion. The two steps are performed as smooth transitions from hover to hover with a peak helicopter velocity of 2 m/s. The simulated vs measured helicopter motion is shown in Fig. 19, and it can be seen that the previously mentioned attractor is making sure that the modeled response is following the broad lines of the measured response for the helicopter. On the right side of Fig. 19, we can see the comparison between measured and modeled slung-load horizontal velocities, and it is clear that there is very good agreement between the two. The discrepancies around 15 s and again around 35 s on the longitudinal slung-load motion originates from the attitude estimation errors with large roll angles that are reflected in the mapping of the slung-load position measurement from the vision system.

B. Dual-Wire Suspension System

Here, the model is validated against data from a test flight with the dual-wire suspension system. The flight consists of the helicopter flying in a square, as illustrated in Fig. 20 with both modeled and measured slung-load position plotted. Figure 21 shows a comparison between modeled and measured slung-load translational and rotation velocities. It can be seen that the model has captured the general motion response of the system well, but, naturally, the position discrepancies grow with time as the errors are integrated.

X. Conclusions

In this paper, a generic slung-load model was presented, capable of modeling all body-to-body suspension types. The model was derived using the Udwadia–Kalaba equation and a redundant coordinate formulation in which the wires were inserted as acceleration constraints. The model was augmented with the ability to detect and respond to the slackening and tightening of wires in a dynamic way, using simple impulse based tightening theory. Furthermore, it was shown how the model could easily be extended to include multilift systems in a generic way for multiple helicopters and loads. The aerodynamic coupling between the helicopter and the load was introduced into the model by calculating the rotor downwash affect on the load. A simple numerical correction scheme was derived for use with the redundant coordinate model. Through two examples, a few of the abilities of the model were shown, both its ability to model different suspension systems and its ability to handle transitions between slack and taut wires. The model was successfully verified against flight data using two different suspension systems.

References

[1] Poli, C., and Cromack, D., "Dynamics of Slung Bodies Using a Single-Point Suspension System," *Journal of Aircraft*, Vol. 10, No. 2, 1973, pp. 80–86. doi:10.2514/3.60200

[2] Prabhakar, A., "Stability of a Helicopter Carrying an Underslung Load," *Vertica*, Vol. 2, No. 2, 1978, pp. 121–143.

[3] Sampath, P., "Dynamics of a Helicopter-Slung Load System," Ph.D Thesis Univ. of Maryland, College Park, MD, 1980.

[4] Ronen, T., Bryson, A. E., and Hindson, W. S., "Dynamics of a Helicopter with a Sling Load," *AIAA Atmospheric Flight Mechanics Conference*, AIAA Paper 86-2288, 1986.

[5] Cicolani, L. S., and Kanning, G., "Equations of Motion of Slung-Load Systems, Including Multilift Systems, NASA, TP-3280, 1992.

[6] Glauert, H., "The Stability of a Body Towed by a Light Wire," Great Britain Aeronautical Research Committee Rept. & Memo 1312, 1930.

[7] Lucassen, L. B., and Sterk, F. J., "Dynamic Stability Analysis of a Hovering Helicopter with a Sling Load," *Journal of the American Helicopter Society*, Vol. 10, April 1965, pp. 6–12.

[8] Fusato, D., Guglieri, G., and Celi, R., "Flight Dynamics of an Articulated Rotor Helicopter with an External Slung Load," *Journal of the American Helicopter Society*, Vol. 39, No. 4, 2002, pp. 577–586.

[9] Micale, E. C., and Poli, C., "Dynamics of Slung Bodies Using a Rotating Wheel for Stability," *Journal of Aircraft*, Vol. 10, No. 12, 1973, pp. 760–763. doi:10.2514/3.60303

[10] Feaster, L., Poli, C., and Krichho, R., "Dynamics of a Slung Load," *Journal of Aircraft*, Vol. 14, No. 2, 1977, pp. 115–121. doi:10.2514/3.44578

[11] Cicolani, L. S., Kanning, G., and Synnestvedt, R., "Simulation of the Dynamics of Helicopter Slung Load Systems," *Journal of the American Helicopter Society*, Vol. 40, No. 4, 1995, pp. 44–61.

[12] Stuckey, R. A., "Mathematical Modelling of a Helicopter Slung-Load Systems," Defence Science and Technology Organisation, Air Operations Division Aeronautical and Maritime Research Lab. Technical Rept., Victoria, Australia, 2002.

[13] Udwadia, F. E., and Kalaba, R. E., "A New Perspective on Constrained Motion," *Proceedings: Mathematical and Physical Sciences*, Vol. 439, No. 1906, 1992, pp. 407–410.

[14] Udwadia, F. E., "Equations of Motion for Mechanical Systems: A United Approach," *International Journal of Non-Linear Mechanics*, Vol. 31, No. 6, 1996, pp. 951–958. doi:10.1016/S0020-7462(96)00116-3

[15] Hughes, P. C., *Spacecraft Attitude Dynamics*, Wiley, New York, 1986.

[16] Curtiss, J. H. C., "Studies of the Dynamics of the Twin-Lift System," NASA, CR-183273, 1988.

[17] Chen, R. T. N., "A Survey of Non-Uniform Inflow Models for Rotorcraft Flight Dynamics and Control Applications," *Vertica*, Vol. 14, No. 2, 1990, pp. 147–184.

[18] Ascher, U. M., Chin, H., Petzold, L. R., and Reich, S., Stabilization of Constrained Mechanical Systems with DAEs and Invariant Manifolds, *Mechanics of Structures and Machines*, Vol. 23, No. 2, 1995, pp. 135–158. doi:10.1080/08905459508905232

[19] Baumgarte, J., "Stabilization of Constraints and Integrals of Motion in Dynamical Systems," *Computer Methods in Applied Mechanics and Engineering*, Vol. 1, No. 1, 1972, pp. 1–16. doi:10.1016/0045-7825(72)90018-7

[20] Civita, M. L., "Integrated Modeling and Robust Control for Full-Envelope Flight of Robotic Helicopters," Ph.D Thesis, Carnegie Mellon Univ., Pittsburgh, PA, 2002.

[21] Talbot, P. D., Tinling, B. E., Decker, W. A., and Chen, R. T. N., "A Mathematical Model of a Single Main Rotor Helicopter for Piloted Simulation," NASA, TM 84281, 1982.